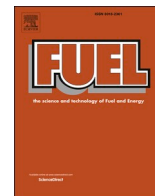




Contents lists available at ScienceDirect

Fuel

journal homepage: [www.elsevier.com/locate/fuel](http://www.elsevier.com/locate/fuel)

## Full Length Article

# Experimental investigation of hydrous ethanol/air flame front instabilities at elevated temperature and pressures

Luis Fernando Marcondes Gárzon Lama<sup>a,b</sup>, Loreto Pizzuti<sup>c</sup>, Julien Sotton<sup>b</sup>,  
Cristiane A. Martins<sup>a,\*</sup>

<sup>a</sup> Instituto Tecnológico de Aeronáutica - ITA, São José dos Campos, SP 12228-900, Brazil

<sup>b</sup> Institut PPRIME, CNRS/ISAE-ENSMA/Université de Poitiers, France

<sup>c</sup> Federal University of ABC, UFABC, Av. dos Estados, 5001, Santo André 09210-580, Brazil

## ARTICLE INFO

## Keywords:

Cellular instability  
Hydrous ethanol  
Hydrodynamic instability  
Diffusional-thermal instability  
Laminar burning velocity

## ABSTRACT

The present work experimentally investigates hydrous ethanol/air flame stability. The experimental data were obtained using spherically expanding flames in a constant volume bomb with optical access for high-speed schlieren photography. It explores the effect of flame parameters, such as thermal expansion rate, flame thickness, activation energy, and effective Lewis numbers, on flame dynamics at elevated pressures (2 to 6 bar) and temperatures (380 and 450 K), at various equivalence ratios (0.6 to 1.3) and water dilution contents (0, 5, 20 and 30% in volume). Adding water to the ethanol/air mixture and increasing its content leads to a significant decrease in flame instability, reducing the thermal expansion ratio while increasing the flame thickness and therefore reducing the propensity of hydrodynamic instability appearance on the flame front. The equivalence ratio has a significant effect on flame stability as well. Slightly rich mixtures present the maximum thermal expansion ratio and minimum flame thickness, therefore, presenting the highest propensity for hydrodynamic instability of the flame front. Besides, the effective Lewis number significantly decreases with equivalence ratio, showing a higher propensity of diffusional-thermal instability for rich mixtures. The flame front instability significantly increases with the mixture initial pressure, which results from the enhancement of the hydrodynamic instability due to the significant decrease in the flame thickness for all equivalence ratios. The initial temperature has a weaker effect on flame stability compared to the other thermo-chemical properties investigated. However, the flame front instability slightly increases with temperature.

## 1. Introduction

Nowadays, due to the increasing concern on environmental pollution and global warming, more stringent emission regulations and the issue of the rapid depletion of fossil fuels, biofuels are increasingly gaining the interest of governments and researchers for their application in internal combustion engines (ICEs) [1,2]. The first four aliphatic alcohols, i.e. methanol, ethanol, propanol, and butanol, are of interest as fuels because they have characteristics that allow them to be used in ICEs and can be synthesized biologically from biomass [3]. Ethanol, produced from sugarcane or corn, presents lower production costs compared to the other first four aliphatic alcohols and therefore, it is the largest used biofuel in current production ICEs [4,5]. Ethanol has a higher octane number, higher laminar burning velocity (LBV), and wider flammability limits, which represent advantages when compared to gasoline. On the

other hand, ethanol has higher latent heat than gasoline, shows cold-start difficulties, and poor diffusion, eventually leading to incomplete combustion [6,7]. A substantial reduction in distillation costs (from 37% to 3%) and an improvement in the net energy gain from 21% to 55% of the energy from ethanol and coproducts are obtained when hydrous ethanol is used instead of anhydrous ethanol [8]. In recent years, researchers investigated the use of hydrated ethanol in practical engines. Fagundez et al. [9] reported an experimental study using an SI engine fueled by hydrous ethanol. They tested different experimental conditions and indicated that optimal efficiency was achieved with an ethanol–water composition containing 30% water. Other researchers investigated the direct use of wet ethanol in homogeneous charge compression ignition (HCCI) engines for power generation. They used exhaust heat recovery to achieve autoignition and stable combustion of wet ethanol containing up to 30% water [10,11].

Laminar burning velocity is used to predict the turbulent flame speed

\* Corresponding author.

E-mail address: [cmartins@ita.br](mailto:cmartins@ita.br) (C.A. Martins).

<https://doi.org/10.1016/j.fuel.2020.119555>

Received 13 July 2020; Received in revised form 15 October 2020; Accepted 17 October 2020

0016-2361/© 2020 Elsevier Ltd. All rights reserved.

**Nomenclature**

$A$	Flame Surface Area
$\mathcal{A}$	Mixture's Strength
$D_{i,mix}$	Mass Diffusivity
$(dT/dx)_{max}$	Maximum Gradient of Temperature
$E$	Activation Energy
$Le$	Lewis Number
$L_b$	Markstein Length
$Le_i$	Individual Species Lewis Number
$Le_{eff}$	Effective Lewis Number
LBV	Laminar Burning Velocity
$l_f$	Flame Thickness
$M_i$	Single Reactant
OPF	Outwardly Propagating Flame
$P_0$	Initial Pressure
$\mathcal{R}$	Universal Gas Constant
$R$	Flame Radius
$R_f(t)$	Flame Front Radius Evolution
$R_{cr}$	Critical Radius
$S_b$	Flame Propagation Speed
$S_b^0$	Unstretched Flame Propagation Speed

SCOP	Spherical Chamber with OPTical access
$S_L$	Laminar Burning Velocity
$T_u$	Initial Temperature
$T_b$	Adiabatic Flame Temperature
$v/v$	Volume/Volume
$W$	Water Content
$Y$	Mass Fraction

**Greek Symbols**

$\alpha$	Thermal Diffusivity
$\beta$	Zeldovich number
$\kappa$	Stretch Rate
$\rho_u$	Unburned Mixture Density
$\rho_b$	Burned Mixture Density
$\sigma$	Thermal Expansion Ratio
$\nu_i$	Stoichiometric Coefficient
$\phi$	Equivalence Ratio
$\chi$	Molar Fraction

**Subscripts**

$D$	Deficient Reactant
$E$	Excess Reactant

in combustion simulation whereas the flame front instability is important to understand the transition from laminar to turbulent combustion [12–17]. Moreover, particularly in premixed flames, a coagulated flame front due to the formation of cellular instabilities could induce the turbulence of unburned mixture and subsequently the rapid increase in flame propagation velocity, which could be one of the main reasons for gas explosion [18]. Thus, the investigation of the fundamental laminar combustion characteristics, principally LBV and flame surface instability, are of great interest for ethanol application as a fuel in ICEs.

Ethanol LBV has been investigated over the last forty years since Gulder's work [19] and is possible to find quite a large amount of data, principally concerning the mixture of ethanol/air [15,20–24] and ethanol-iso-octane blends [25–28]. On the other hand, for the mixture of ethanol-water/air, fewer data are available [29–31]. Regarding flame surface instability, only a small number of investigations have focused on the flame stability of alcohol fuels. Among them were Zhang et al. [14] who studied flame instability of methanol/air mixtures diluted with CO<sub>2</sub> and N<sub>2</sub> at initial temperatures,  $T_u$ , from 310 to 410 K and initial pressures,  $P_0$ , from 0.1 to 0.5 MPa. They found that the Markstein length, and therefore flame front stability, increases monotonously with the increase in equivalence ratio,  $\phi$ , except for  $\phi$  less than 0.8, and decreases with the increase in  $T_u$  and  $P_0$ . Besides, mixture dilution increases the sensitivity of the flame front to the flame stretch rate. Wang et al. [32] studied the flame instability of methanol/air mixtures at  $P_0$  up to 10 atm,  $T_u$  of 373 and 423 K and  $\phi$  between 0.7 and 2.1, reporting that cellular instability monotonically increases with increasing  $T_u$  or  $P_0$  and non-monotonically varies with increasing  $\phi$ , and that, under very rich conditions, the critical flame radius raises increasing  $\phi$ . Gu et al. [33] and Li et al. [34] investigated flame instability at high pressures and temperature of *tert*-butanol-air ( $\phi$  between 0.8 and 1.5) and methyl-1-butanol-air ( $\phi$  between 0.6 and 1.8) mixtures, respectively. Both groups found that the flame front instability increases with the increase in  $\phi$  and  $P_0$  while being almost insensitive to the  $T_u$ . Gas-phase ethanol-air mixtures flame instability has been investigated by [35] for anhydrous ethanol at  $P_0$  up to 1.4 MPa and  $T_u$  of 393 K. The Markstein number decreases with pressure and increases slightly with temperature with these tendencies being more pronounced for richer mixtures. More recently, ethanol and hydrous ethanol/air (the azeotropic mixture) aerosols flame instabilities have been investigated by Bradley et al. [16]. They found that the presence of fuel droplets, at a given value of  $\phi$ ,

enhances the generation of both hydrodynamic and thermo-diffusive instabilities, decreasing the critical Peclet number for their onset.

In this way, bearing in mind the importance of ethanol as a renewable fuel in the global context and the scarcity of experimental data regarding ethanol combustion characteristics, particularly for hydrous ethanol, the current research is a follow-up to the previous work by the authors [31]. The focus of that work was the experimental determination of LBV of wet ethanol with water content,  $W$ , from 0 up to 30% v/v. Fig. 1 provides a brief plot with the previous results of LBV. It was qualitatively presented that the onset of instability occurs at higher  $P_0$  or larger radii as the water content increases, but without providing details or any quantitative results. The present study aims to improve the understanding of instability in anhydrous and hydrous ethanol premixed flames, quantitatively analyzing the effects of thermo-chemical properties ( $P_0$ ,  $T_u$ ,  $\phi$  and  $W$ ) on the Markstein length and the most significant parameters controlling hydrodynamic and diffusional-thermal instabilities. The thermochemical properties are  $T_u$  of 380 and 450 K,  $P_0$  from 1 to 6 bar,  $\phi$  between 0.6 and 1.3 and 0, 5, 10, 20, and 30% water by volume in ethanol. Also, the flame morphology based on the trends of these parameters is presented and discussed. Finally, some critical radii obtained from experimental data are presented.

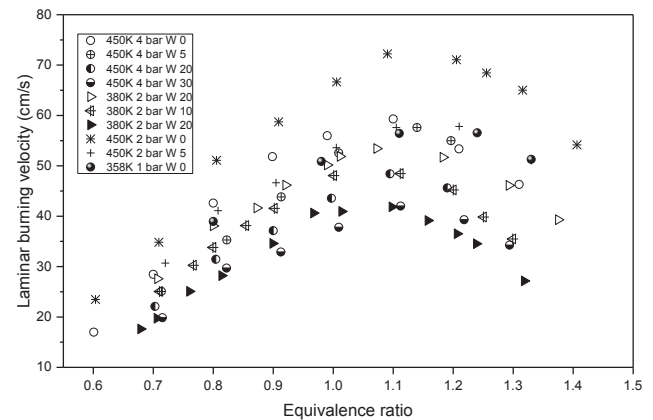


Fig. 1. Laminar burning velocity, a brief plot from the previous work by the authors [31]

## 2. Laminar flame instability

It is well known from experiments that even when a flame propagates in a quiescent mixture, the front eventually becomes unstable due to its intrinsic instabilities. If the flame front outgrows the disturbances experienced the disturbance appears to decay relative to the flame, leading to flame stability. Conversely, when the disturbance grows at a faster rate than the flame, instability results [36]. According to [37], observation of cellular flames in combustible mixtures extends back to early measurements of polyhedral flames in 1892 by Smithells and Eingel. Previous studies [38–40] reported three main types of flame surface instabilities that can be observed during experiments: hydrodynamic, diffusional-thermal, and body-force instabilities.

The hydrodynamic, or Darrieus-Landau instability, first recognized by George Darrieus and Lev Landau [41,42], is the most prominent intrinsic flame instability which results from the gas expansion produced by the heat released from the exothermal reactions of combustion [43]. Perturbations of the flame front are enhanced by the hydrodynamic disturbances induced by the gas expansion. Therefore, the hydrodynamic instability primarily depends on the thermal expansion ratio across the flame.

The non-equal diffusion process between the heat-conducting away from the reaction zone and reactant mass diffusing towards the reaction zone is responsible for the diffusional-thermal instability. The effect of non-equi-diffusion can be assessed by the Lewis number ( $Le$ ), defined as the ratio of mixture thermal diffusivity to mass diffusivity of the limiting reactant relative to abundant inert gas [18,44,45]. If  $Le$  is larger than unity, the heat diffusion is the preponderant parameter in the propagation mechanism and the flame will be thermo-diffusively stable. Conversely, if  $Le$  less than 1, the flame is thermo-diffusively unstable [46].

Buoyancy driven (or body-force) instability, commonly known as the Rayleigh–Taylor instability, which leads to flame surface distortion from a spherical shape, deflecting the flame boundary upwards from the location of the spark kernel, is only observed when LBV is small, lower than 15 cm/s [39,47]. In this work, the mixture laminar burning velocities are always larger than 15 cm/s, therefore, buoyancy driven instability can be neglected, and only combined effects of hydrodynamic and diffusional-thermal instabilities are taken into account.

An important role in flame instability is played by the flame stretch rate, which accounts for curvature and aerodynamic effects in outwardly propagating flames (OPF). According to [47] and [48], the strong effect of flame stretch (large curvature) at the early stage of flame propagation suppresses the hydrodynamic instability and therefore the diffusional-thermal instability plays a dominant role in the flame stability. As observed by [49], except for very intense turbulence, the early instants of kernel expansion are laminar due to the increase in viscosity with temperature, the small size of the kernel, and the very short deposit duration. With the increase in flame radius, the flame stretch decreases, as curvature decreases, weakening its inhibiting effect on hydrodynamic instability; therefore, both diffusional-thermal and hydrodynamic instabilities determine the flame front stability at later stages, [47,48].

The hydrodynamic instability is therefore strongly dependent on the flame thickness, in addition to the thermal expansion ratio. The thinner flame will reduce the influence of curvature and enhance the baroclinic torque intensity, therefore enhancing the destabilizing propensity of the flames [18,50].

### 2.1. Parameters involved in the cellular instability analysis

#### 2.1.1. Thermal expansion ratio and flame thickness

Thermal expansion ratio ( $\sigma$ ) and flame thickness ( $l_f$ ) are the most sensitive parameters controlling the hydrodynamic instability [51]. The thermal expansion ratio is defined in Eq. (1) as the ratio of unburned to burned mixture density and is calculated using the Cantera software [52]:

$$\sigma = \frac{\rho_u}{\rho_b} \quad (1)$$

The flame thickness is determined based on the gradient method given in Eq. (2), where  $T_b$  and  $(dT/dx)_{max}$  are the adiabatic flame temperature and the maximum gradient of temperature, respectively.

$$l_f = \frac{T_b - T_u}{(dT/dx)_{max}} \quad (2)$$

Fig. 2 shows the way  $(dT/dx)_{max}$  is determined for pure ethanol/air mixture at  $P_0 = 2$  bar and  $T_u = 450$  K using the Chemkin-Pro® software [53].

#### 2.1.2. Formulations for $Le$ and $Le_{eff}$ determination

The Lewis number ( $Le$ ) is defined as the ratio of the thermal diffusivity to the mass diffusivity of the deficient reactant. The deficient reactant is the fuel species for lean mixtures and oxidizer species for rich mixtures, respectively. The individual species Lewis number ( $Le_i$ ) is given by Eq. (3), where  $\alpha$  is the thermal diffusivity of the fuel–air–diluent (ethanol–air–water) mixture and  $D_{i,mix}$  is the mass diffusivity calculated using Eq. (4) where  $Y$  is the mass fraction and  $\chi$  the molar fraction of each species,  $s$ , in the mixture [53–54].

$$Le_i = \frac{\alpha}{D_{i,mix}} \quad (3)$$

The Lewis number of the mixture is obtained taking into consideration that ethanol is the only fuel and oxygen is the only oxidizer whereas  $H_2O$  and  $N_2$  are treated as diluents.

$$D_{i,mix} = (1 - Y_{i,mix}) \left( \sum_{s=1}^N \frac{\chi_s}{D_{i,s}} \right)^{-1} \quad (4)$$

The individual species  $Le$  is calculated using the Colorado State University (CSU) online program [55] where all properties are evaluated using the Chemkin® Collection [53].

Two analysis have been conducted considering the Lewis number. The first considers only the  $Le$  of the deficient reactant in the mixture for each experimental condition ( $P_0$ ,  $T_0$ ,  $\phi$ ,  $\chi_{H_2O}$ ) according to Eq. (3). The second analysis follows that of [56] where the chemical reaction is defined according to Eq. (5) by a single overall irreversible global reaction step with two reactants.



The subscripts  $D$  and  $E$  stand for the deficient and the excess reactant, respectively, the chemical symbol  $M_i$  represents the single reactant and  $\nu_i$  its stoichiometric coefficient. The chemical reaction orders are taken

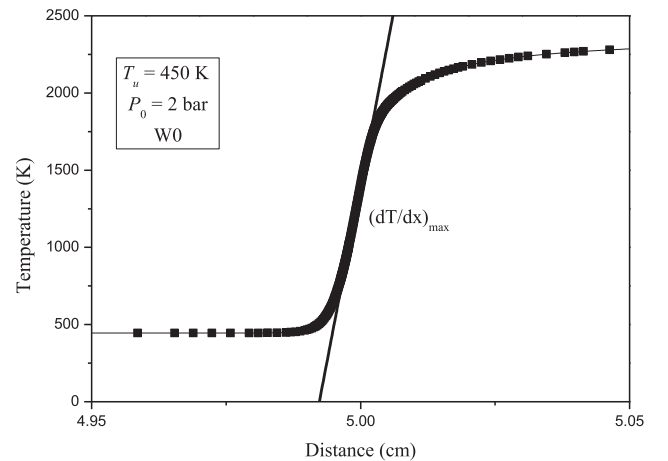


Fig. 2. Graphical representation of  $(dT/dx)_{max}$  calculation for pure ethanol/air mixture.

to be unity. The mixture is characterized by two distinct Lewis numbers  $Le_D$  and  $Le_E$  calculated using the CSU online program. According to [56,57]  $Le_D$  and  $Le_E$  combine into a single effective Lewis number,  $Le_{eff}$ , given in Eq. (6).

$$Le_{eff} = 1 + \frac{(Le_E - 1) + (Le_D - 1)\mathcal{A}}{1 + \mathcal{A}} \quad (6)$$

where  $\mathcal{A} = 1 + \beta(\Phi - 1)$  is a measure of the mixture's strength. The parameter  $\Phi$  is always defined as larger than one; it is equal to the equivalence ratio,  $\phi$ , for fuel-rich mixtures, and its reciprocal for fuel-lean mixtures [56]. is the Zeldovich number defined in Eq. (7) where  $\mathcal{R}$  is the universal gas constant [58] and  $E$  the activation energy which can be determined from Eq. (8) [59].

$$\beta = E \frac{(T_b - T_u)}{\mathcal{R}T_b^2} \quad (7)$$

$$\frac{E}{\mathcal{R}} = -2 \frac{d \ln(\rho_b S_L)}{d(1/T_b)}$$

The evaluation of  $E/\mathcal{R}$  requires the calculation of  $\rho_b S_L$  at different  $T_b$ . The laminar burning velocity,  $S_L$  is numerically estimated by small variations of  $T_u$  in the  $T_u \pm 5$  K range according to [60] and the adiabatic flame temperature was calculated using the Chemkin® FLAME SPEED CALCULATOR [53] package. A test with a larger variation of  $T_u$  ( $T_u \pm 10$  K) was conducted for comparison, showing a maximum difference of 0.72% at  $T_u = 450$  K,  $P_0 = 4$  bar and W0, as presented in Table S2 of the supplementary material.

The Markstein length,  $L_b$ , a global flame parameter which quantifies the flame response to the total flame stretch rate, was determined by using the linear relationship between the flame propagation speed  $S_b$  and the stretch rate  $\kappa$  given by  $S_b = S_b^0 - L_b \kappa$ . The flame front radius evolution,  $R_f(t)$ , is derived from the flame images obtained using high-speed schlieren photographic techniques. The flame propagation speed,  $S_b$ , which is subject to stretch, is calculated by  $S_b = dR_f/dt$ . The flame total stretch rate,  $\kappa$ , is defined in Eq. (9), according to [38], where  $A$  corresponds to the flame surface area.

$$\kappa = \frac{1}{A} \frac{dA}{dt} = \frac{2}{R_f} \frac{dR_f}{dt} = \frac{2}{R_f} S_b \quad (9)$$

The unstretched flame propagation speed,  $S_b^0$ , is obtained from the  $S_b$ - $\kappa$  graph using a linear extrapolation method and the laminar burning velocity is obtained applying the continuity equation  $S_L = \frac{\rho_b}{\rho_u} S_b^0$ . The reliability of the linear method for the conditions under analysis in this work is explained in [31] and presented in Table S3 of the supplementary material.

Even though for some mixtures  $E/R$  is almost the same for  $\phi$  between 0.8 and 1.0 [50], for the mixtures under analysis it was found significant variations for this parameter. Therefore, the was calculated using the specific  $E/R$  value for each mixture composition and initial conditions, whose values and tendencies are presented in Table S1 and Figs. S1 and S2 of the supplementary material.

For lean and rich mixtures, the effective Lewis number tends towards the  $Le$  of ethanol and oxygen, respectively. It is a monotonically decreasing function as the equivalence ratio increases from lean to rich. The limiting  $Le_{eff}$  of the fuel and the oxidizer are calculated as 1.7216 and 0.9338, according to Table S1. The highest value is obtained for  $T_u = 450$  K,  $P_0 = 4$  bar,  $\phi = 0.6$  and W30, i.e. the maximum water content in the leanest condition. On the other hand, the lowest value is obtained for  $T_u = 450$  K,  $P_0 = 4$  bar,  $\phi = 1.3$ , and W0, i.e. pure ethanol in the richest condition.

### 2.1.3. Critical radius

In spherical propagating flames, most researchers consider two instants at which the cell morphology characteristics change [51,56,61–64]. The first is when the large cracks formed from the spark discharge lose self-similarity and show initial cross-cracking, however, no influence on the flame propagation speed is observed. The second

moment is when cells, smaller than the branched cracks, appear spontaneously and uniformly over the entire flame surface, associated with a significant increase in flame speed. In this study, the second moment is used to define the onset of flame instability and is represented by the critical radius,  $R_{cr}$ . The critical radius is obtained from the plot of the stretched flame velocity versus the flame stretch rate. In this case,  $R_{cr}$  is detected at the moment when the burning velocity increases significantly and loses the linear relationship between the stretched flame velocity and the flame stretch rate [34,63].

## 3. Experimental setup

The experiments described in the present study were conducted in the Institut Pprime of ISAE-ENSMA, France. The experimental facility, known as SCOP (Spherical Chamber with OPTical access), is a spherical stainless-steel closed vessel that enables the determination of stretched laminar flame speeds and the associated Markstein lengths of outwardly propagating spherical flames. Two types of fuels, gaseous or liquid, can be used. The radius of the inner spherical stainless-steel bomb is 200 mm ( $\approx 4.2$  L) and the maximum initial operating pressure and temperature are limited to 1 MPa and 470 K, respectively. The maximum absolute error for  $T_u$  before an explosion is estimated at  $\pm 2.2^\circ$  C. The optical access is provided through two 70 mm diameter sapphire UV windows. Other aspects of the equipment and experimental technique have been described in detail by Dortz et al. [65]. Their work was the first conducted in SCOP; it was utilized to determine the LBV of kerosene surrogate fuel mixtures. Subsequently, the SCOP installation was used in the previous work of Lama et al. [31] which focused on the LBV determination of hydrous ethanol. In this previous work, there is a description of the considerable preparatory work and all details regarding the preparation of ethanol–water/air–fuel mixtures and the experimental protocol applied during the tests. The same procedures were applied during the present tests.

For the present work, the main goal is the study of cellular instability in hydrous ethanol flame. Thus, images of spherical flames propagating in quiescent premixtures were captured using high-speed Schlieren photography at 7000 frames per second at different initial conditions of pressures, temperatures, stoichiometry, and water content where the onset of flame instability and associated flame acceleration is perceived. The error for the radii of the flames determined from a schlieren image arises from the resolution of the digital camera and the uncertainty of the flame diameter was calculated to be less than 0.19%. The error for the schlieren time is assumed to be negligible.

For the measurements at 1, 2, 4, 5 and 6 bar the errors for the starting pressure were 0.65, 1.6, 0.8, 0.6, and 0.4%, respectively as two different pressure transducers were used, one for pressure up to 2 bar and the other for higher pressures. Regarding error uncertainties, Dortz [66] performed an extensive analysis of the experimental setup employed. However, for the cases under analysis, there is a relative uncertainty lower than 1.4%, regarding the mixtures equivalence ratio. The maximum error in the proportion of ethanol and water blend, considering the error produced by the syringe in each injection was under 0.21%. The uncertainty regarding the unstretched laminar flame speed was around 8% in average, reaching a maximum value of 14% in more extreme conditions such as  $P_0 = 5$  bar, especially due to the flame front instabilities, which imply in more scattered points resulting in larger uncertainties in the extrapolation method. Conditions of  $\phi = 0.6$  could not be seen in all cases since the post-processing needs a minimum value of flame propagation speed to extrapolate results. The experimental conditions are presented in Table 1.

## 4. Results and analysis

This section presents the experimentally determined effects of thermo-chemical properties ( $P_0$ ,  $T_u$ ,  $\phi$  and  $W$ ) on the Markstein length,  $L_b$ , and on the most significant parameters controlling hydrodynamic ( $\sigma$



**Table 1**

Experimental conditions investigated in this work.

Fuel Mixtures	$P_0$ [bar]	$T_u$ [K]	Equivalence Ratio, $\phi$
W0 W10 W20 W30	2	380	0.6 0.8 1.0 1.2
W0	2	380 450	1.3
W0 W20	2	450	0.6 0.8 1.0 1.2
W0 W5 W20 W30	4	450	0.6 0.8 1.0 1.2 1.3
W0	6	380 450	1.0
W0 W20	1 3 5	380 450	1.0
W30	5	450	1.0

and  $l_f$ ) and diffusional-thermal ( $Le_{eff}$ ) instabilities. Besides, it is presented and discussed the flame morphology based on the trends of  $\sigma$ ,  $l_f$ , and mixture  $Le_{eff}$ . Finally, it presents the  $R_{cr}$  values obtained from experimental data for the mixtures under analysis that showed the transition to unstable flames within the available experimental data.

#### 4.1. Effect of thermo-chemical properties on the Markstein length

The Markstein length is a global flame parameter, which quantifies the flame response to the total flame stretch rate, including both curvature and aerodynamic strain effects, and reflects the variation of flame instability. For OPF, when  $L_b$  greater than 0, the stretched laminar flame propagation speed,  $S_b$ , increases while decreasing the total stretch rate because when flame propagates, its curvature decreases. In this case, the growth rate of flame front protuberances (cells) is lower than that of flame expansion, thus enhancing the flame front stability [12,18]. Therefore, larger  $L_b$  values suggest that the flame front is less likely to present a wrinkled surface [47]. Conversely, when  $L_b$  less than 0,  $S_b$  decreases while the flame front expands, and the total stretch rate decreases. The growth rate of flame front protuberances is now higher than that of flame expansion, thus enhancing the flame front instability.

Fig. 3 presents the experimentally determined burned gas  $L_b$  for various  $\phi$  at  $P_0$  of 2 and 4 bar and  $T_u = 450$  K and  $P_0 = 2$  bar and  $T_u = 380$  K, marked with open symbols, compared with experimentally determined  $L_b$  values available in the literature, closed symbols, showing reasonable agreement. In this work,  $L_b$  is derived from the gradient of the plot of flame propagation velocity against the stretch rate. However, according to [30] and based on personal experience, measurements of the  $L_b$  are subject to reasonable amounts of scatter. Despite such uncertainty, the general trend is a monotonic decrease of the  $L_b$  with increasing  $\phi$ , for all pressures and temperatures under

analysis. Existing investigations of the Markstein lengths show a much stronger dependence of  $L_b$  on  $\phi$  than on  $P_0$  and  $T_u$ . However, while the mixture pressure increase leads to lower  $L_b$ , consistent trends for temperature dependence are not indicated, confirming Hinton et al. conclusions [30].

Fig. 4 presents the  $L_b$  for various  $\phi$  and water dilutions at  $P_0 = 2$  and 4 bar and  $T_u = 450$  K. Regarding the water content effect on the  $L_b$ , a general trend is not available from the experimental data of this work and no data have been found in the literature for comparison. However, data from  $P_0 = 2$  bar show little increase in the  $L_b$  with water content for lean and stoichiometric mixtures, thereby slightly increasing the flame front stability. On the other hand, for rich mixtures, increasing the water content leads to an  $L_b$  decrease, thus increasing the tendency to flame front instability.

#### 4.2. Effect of thermo-chemical properties on the thermal expansion ratio

The thermal expansion ratio,  $\sigma$ , is one of the most sensitive parameters controlling the hydrodynamic instability [45,51]. Larger values of  $\sigma$  correspond to a higher propensity of hydrodynamic instability appearance on the flame front.

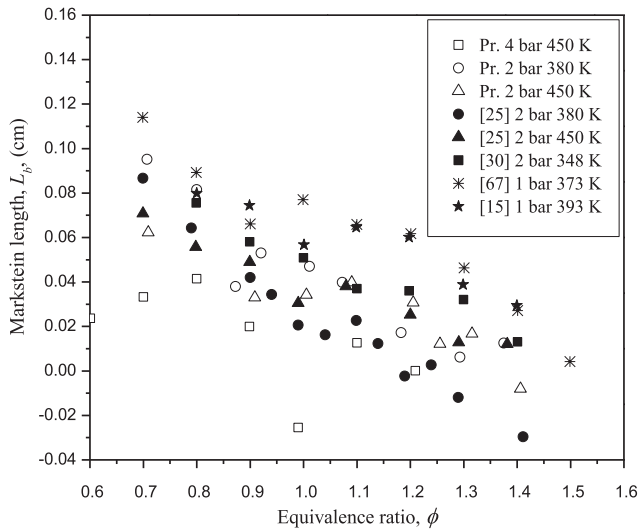
Fig. 5 shows the effect of water dilution on  $\sigma$  for  $\phi$  varying between 0.6 and 1.3, at  $P_0 = 4$  bar and  $T_u = 450$  K. A similar tendency of  $\sigma$  versus  $\phi$  can be observed for all the water contents under analysis, with a peak corresponding to a slightly rich mixture. The increase in water content reduces  $\sigma$ . However, this effect is more pronounced on the rich side.

Fig. 6 shows the effect of initial temperature on  $\sigma$  for  $\phi$  varying between 0.6 and 1.3, at  $P_0 = 2$  bar, and for water contents W0 and W20. The increase in  $T_u$  from 380 K to 450 K leads to a reduction of  $\sigma$  for both water contents under analysis but with a more significant effect on the rich side. Figs. 5 and 6 show that  $\phi$  strongly affects  $\sigma$ , with a non-monotonic trend, reaching a peak for slightly rich mixtures. As will be shown later in Fig. 11,  $\sigma$  is almost insensitive to  $P_0$ .

#### 4.3. Effect of thermo-chemical properties on the flame thickness

Flame thickness,  $l_f$ , along with  $\sigma$ , is the other most sensitive parameter controlling the hydrodynamic instability [45,51]. Smaller values of  $l_f$  correspond to a higher propensity of hydrodynamic instability appearance on the flame front.

Fig. 7 shows the effect of water dilution on  $l_f$  for  $\phi$  varying in the range between 0.6 and 1.3, at  $P_0 = 4$  bar and  $T_u = 380$  K and 450 K. The flame thickness is higher for leaner mixtures, decreases as the mixture



**Fig. 3.** Markstein length for various  $\phi$  at various  $P_0$  and  $T_u$ , obtained in the present work (Pr.) marked with open symbols, compared with  $L_b$  available in the literature [15,25,30,67], closed symbols.

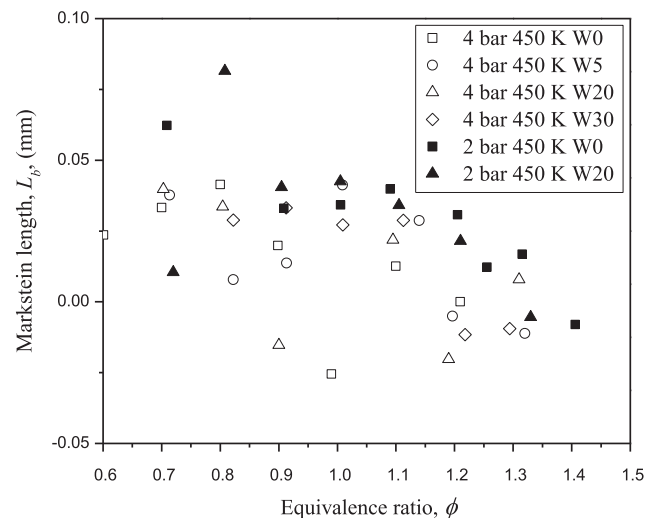


**Fig. 4.** Markstein length for various  $\phi$  and water dilutions at  $P_0 = 2$  and 4 bar and  $T_u = 450$  K.

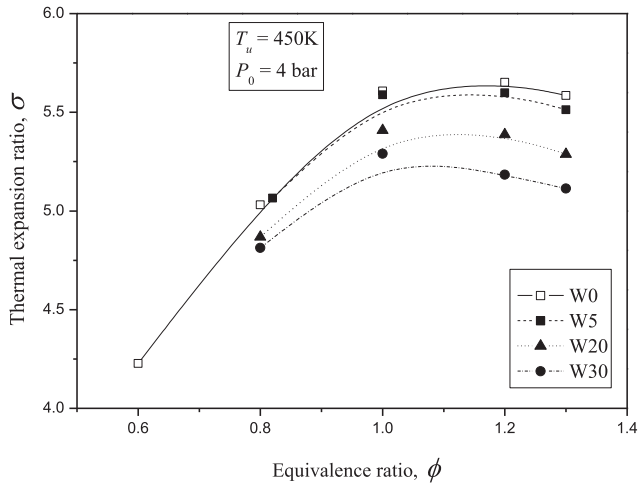


Fig. 5. Thermal expansion ratio at various  $\phi$  and water contents at  $P_0 = 4$  bar and  $T_u = 450$  K.

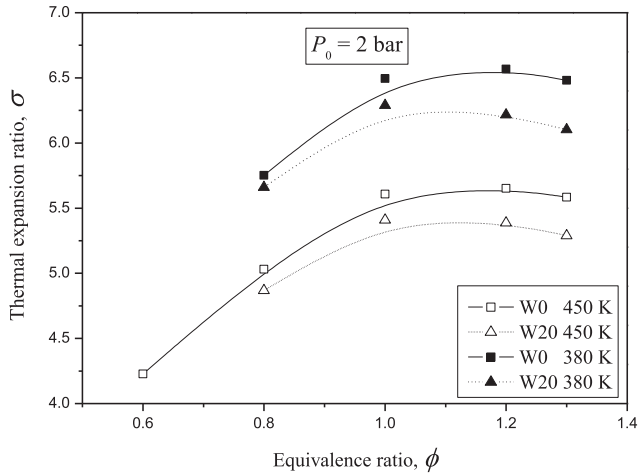


Fig. 6. Thermal expansion ratio at various  $\phi$ ,  $T_u$  and water contents, W0 and W20, at  $P_0 = 2$  bar.

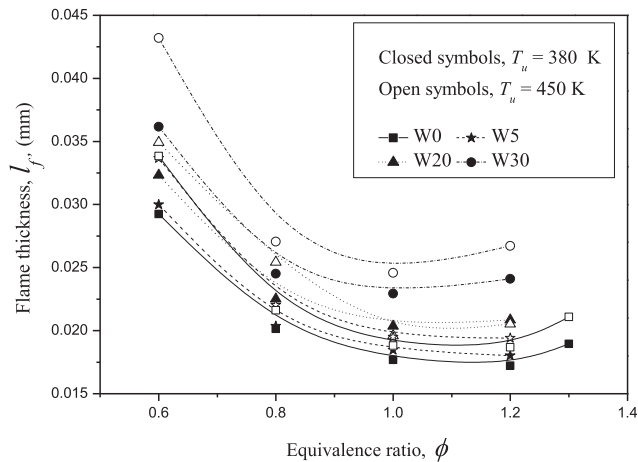


Fig. 7. Flame thickness,  $l_f$ , at various  $\phi$ , water contents and initial temperatures, at  $P_0 = 2$  bar.

tends to stoichiometry and reaches the minimum value for a slightly rich mixture. Any further increase in  $\phi$  leads to an increase in  $l_f$ . This trend is quite similar for different water dilutions; however, increasing the water content of the mixture leads to an increase in  $l_f$ . For the range under consideration, this effect is more pronounced on the rich side. A similar trend is found for both temperatures. However, the flame thickness increases with  $T_u$ .

Fig. 8 shows the effect of water dilution on  $l_f$  for  $P_0 = 2, 4$ , and  $6$  bar, at  $\phi = 1$  and  $T_u = 450$  K. The flame thickness increases almost linearly with the water content under consideration, following a similar trend for all pressures under analysis. However, the increase in  $P_0$  significantly reduces  $l_f$  with a more remarkable decrease at lower pressures.

Analyzing the combined effects of thermo-chemical properties on both  $\sigma$  and  $l_f$  in the range under analysis, it can address their effects on the hydrodynamic instability appearance on the flame front. Increasing the mixture water content leads to a decrease in  $\sigma$  along with an increase in  $l_f$ , leading to a reduction of the propensity of hydrodynamic instability appearance on the flame front. Conversely, higher  $T_u$  is associated with a reduction of  $\sigma$  along with a decrease in  $l_f$ . A not clear effect of  $T_u$  on the hydrodynamic instability of the flame front is therefore available from this analysis. Higher  $P_0$  is associated with a decrease in  $l_f$  with almost no effect on  $\sigma$ , therefore leading to an increase in the propensity of hydrodynamic instability. Regarding the equivalence ratio, the opposite trend is found for  $\sigma$  and  $l_f$ . Lean mixtures have low  $\sigma$  and high  $l_f$ . Increasing  $\phi$ ,  $\sigma$  increases while  $l_f$  decreases, reaching a maximum and minimum value, respectively, at almost the same value of  $\phi$ . For richer mixtures the trend inverts. Therefore, a not clear effect of  $\phi$  on the hydrodynamic instability of the flame front is available from this analysis.

#### 4.4. Effect of thermo-chemical properties on the effective Lewis number

The effective Lewis number,  $Le_{eff}$ , as defined in section 2.2, is the parameter controlling the diffusional-thermal instability caused by the competition between the effects of heat-conducting away from the reaction zone and mass diffusing towards it [47].

Fig. 9 gives  $Le_{eff}$  of ethanol/air mixtures at various water contents  $\phi$  and  $T_u$ .  $Le_{eff}$  shows a slight linear increase with the water content for all mixture  $\phi$  and  $T_u$  under analysis. Therefore, the mixture of water content increase is associated with a more diffusional-thermal stable flame.  $Le_{eff}$  significantly decreases with the increase in  $\phi$ , which implies that the diffusional-thermal instability of ethanol/air flames can be suppressed by decreasing  $\phi$ . Conversely,  $Le_{eff}$  slightly decreases with mixture temperature and this effect is more pronounced for leaner mixtures.

Fig. 10 gives  $Le_{eff}$  of ethanol/air mixtures at various equivalence ratios,  $P_0 = 2$  bar and  $4$  bar, and W20 water contents at  $T_u = 450$  K. Confirming data presented in Fig. 9,  $Le_{eff}$  significantly decreases with the

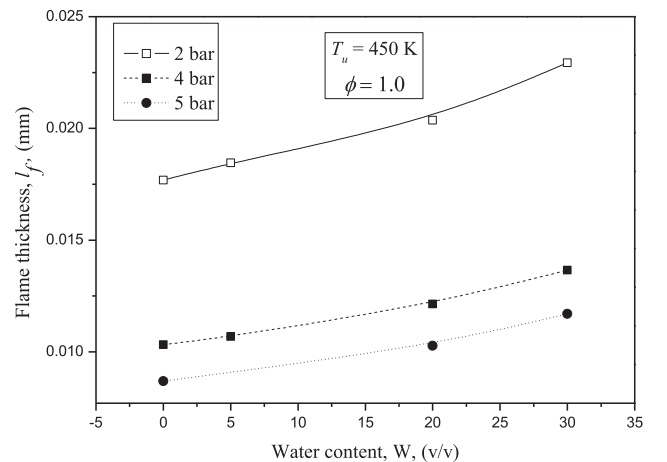
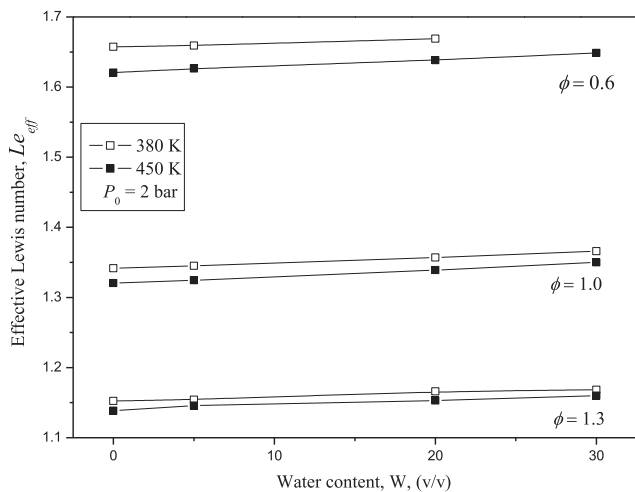
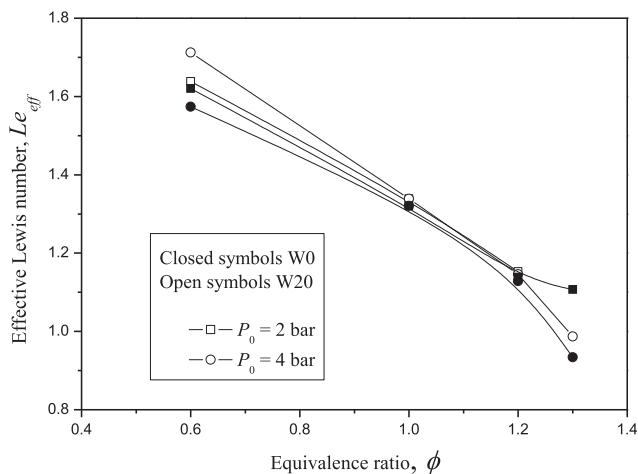


Fig. 8. Water content effect on  $l_f$  at  $P_0 = 2, 4$  and  $6$  bar,  $\phi = 1.0$  and  $T_u = 450$  K.



**Fig. 9.** Effective Lewis numbers of ethanol/air mixtures at various water contents, equivalence ratios, and initial temperatures at  $P_0 = 2$  bar.



**Fig. 10.** Effective Lewis numbers of ethanol/air mixtures at various  $\phi$  and  $P_0$  at  $T_u = 450$  K.

increase in  $\phi$ . It is seen that the effective Lewis number of stoichiometric mixtures is little affected by  $P_0$ . However, for non-stoichiometric mixtures,  $Le_{eff}$  decreases while increasing the mixture  $P_0$ ; this effect is more significant as the equivalence ratio gets further away from stoichiometry and it presents the highest significance on the rich side, for mixtures with  $\phi = 1.3$ . Stoichiometric and lean ethanol/air mixtures present a  $Le_{eff}$  quite larger than unity. The increase of  $T_u$  and  $P_0$  only slightly affects  $Le_{eff}$  in the range under analysis; therefore, diffusional thermal instabilities are suppressed in the lean region. However, they can affect the mixture flame front in rich mixtures, especially at higher mixture pressures. Confirming the results in Fig. 9, it can be seen that the mixture water content, W20, increases  $Le_{eff}$  and this effect is stronger further away from stoichiometry and with increasing mixture  $P_0$ . Therefore, increasing water content in the mixture is associated with a more diffusional-thermal stable flame.

#### 4.5. Flame morphology

The flame traveling the chamber volume may go through various morphological alterations, characterized by the appearance and branching of large cracks and, eventually, fine cellular structures. Fig. 11 shows four images, at selected flame radius,  $R$ , of the sequences of the expanding spherical flame images of stoichiometric ethanol/air

mixtures, W0, at  $T_u = 450$  K and different  $P_0$ , set to 2, 4, and 6 bar, respectively. The  $Le_{eff}$ ,  $\sigma$ , and  $l_f$  are provided on the right of the figure for each mixture. No instabilities appear on the flame surface at  $P_0 = 2$  bar, although some large cracks, that do not develop during the flame propagation, are observed because of ignition disturbances. At  $P_0 = 4$  bar, the flame front remains smooth at the early stages, then some large initial cracks start to branch without reaching a uniform cellular flame surface. However, at  $P_0 = 6$  bar, the entire flame surface becomes covered with uniform cells for a larger flame radius.

Increasing  $P_0$  does not modify the  $Le_{eff}$  of the mixture; therefore, the diffusive-thermal instability is not responsible for the propensity to destabilize the flame front. Therefore, the flame front destabilization should be only addressed to hydrodynamic instability. The two most sensitive parameters controlling the hydrodynamic instability are  $\sigma$  and  $l_f$  [45,51]. The former,  $l_f$ , decreases substantially, whereas the latter,  $\sigma$ , maintains almost the same value with increasing  $P_0$ . Therefore, the increase in cellular instabilities with higher  $P_0$  results from the enhancement of the hydrodynamic instability due to the significant decrease in  $l_f$ .

Fig. 12 shows schlieren images of the sequences of the expanding spherical flame of stoichiometric ethanol/air mixtures, W0, and ethanol-water/air mixtures, (W20 and W30) at  $T_u = 450$  K and  $P_0 = 5$  bar. Uniformly distributed cells appear at later stages, on the flame surface of stoichiometric ethanol/air mixtures. However, in ethanol-water/air mixture, W20, some large initial cracks start to branch without reaching a uniform cellular flame surface. Ethanol-water/air mixture, W30, presents a similar pattern; however, the increase of water content pushes the development of the initial large cracks even further away from the flame center. The water content increase leads to a small increase in the  $Le_{eff}$ , therefore, the diffusive-thermal instability barely reduces the propensity to destabilize the flame front. Additionally, the water content increase leads to a small decrease in the  $\sigma$  and a significant increase in the  $l_f$ . Therefore, the decrease of cellular instabilities with higher water content mainly results from the attenuation of the hydrodynamic instability due to the significant increase in  $l_f$ .

Fig. 13a) and 13b) show schlieren images of the sequences of the expanding spherical flames of stoichiometric,  $\phi = 1.0$ ,  $P_0 = 6$  bar and rich,  $\phi = 1.3$ ,  $P_0 = 2$  bar, respectively, ethanol/air mixtures, W0, at  $T_u = 380$  K and 450 K. The flame front evolution is roughly the same for  $T_u = 380$  K and 450 K. Uniformly distributed cells appear on the flame surface almost at the same flame radius, according to Fig. 13a), whereas, the flame front is a smooth surface although two large cracks are observed in the region of the electrodes because of ignition disturbances, according to Fig. 13b). The  $Le_{eff}$  value is apparently insensitive to  $T_u$ . However, a detailed analysis of Table S1 and Fig. S2 of the Supplementary material shows that the  $Le_{eff}$  is always slightly lower at higher  $T_u$ . Hence, increasing  $T_u$  slightly increases the propensity of diffusional-thermal instabilities. On the other hand, the  $T_u$  increase leads to a decrease in both  $\sigma$  and  $l_f$ . Therefore, the destabilizing effect of the thinner flame front is somehow counterbalanced by the stabilizing effect on hydrodynamic instabilities of smaller  $\sigma$  values. More details on the effect of  $T_u$  on flame stability are presented in section 4.6 when the critical radius is determined based on experimental data.

#### 4.6. Critical radius

The onset of flame instability is represented by the critical radius,  $R_{cr}$ , as defined in section 2.4. Table 2 presents the  $R_{cr}$  values obtained from experimental data at  $P_0 = 2, 4, 5$ , and 6 bar, at  $T_u = 380$  K and 450 K and W0. Only  $R_{cr}$  values for stoichiometric ethanol/air mixture are presented because, for all other water dilution contents under analysis, the critical radius is larger than the optical window radius, according to Fig. 4.8. Therefore, these results confirm that even small concentrations of water in ethanol/air mixtures have a stabilizing effect, thus increasing the critical radius. The critical radius decreases with the increase in  $P_0$  because of the flame thickness decrease. Furthermore, the  $R_{cr}$  decreases

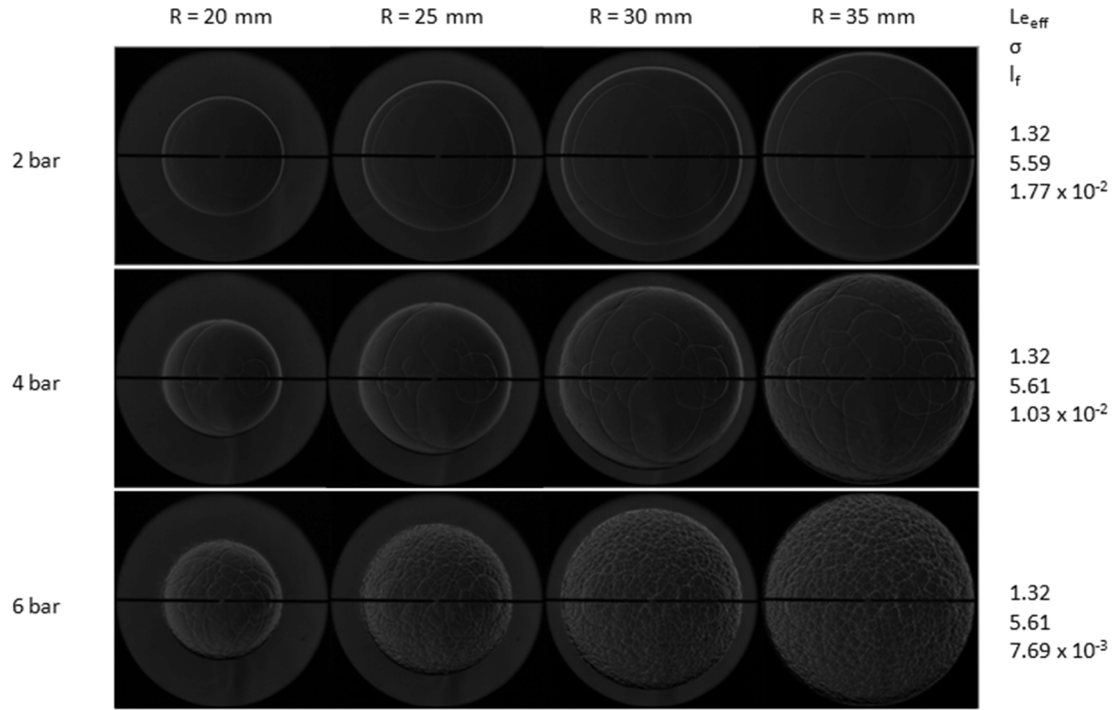


Fig. 11. Schlieren images of stoichiometric ethanol/air mixture, W0, flame front evolution at  $T_u = 450$  K and  $P_0 = 2, 4, 6$  bar. Optical window radius of 35 mm.

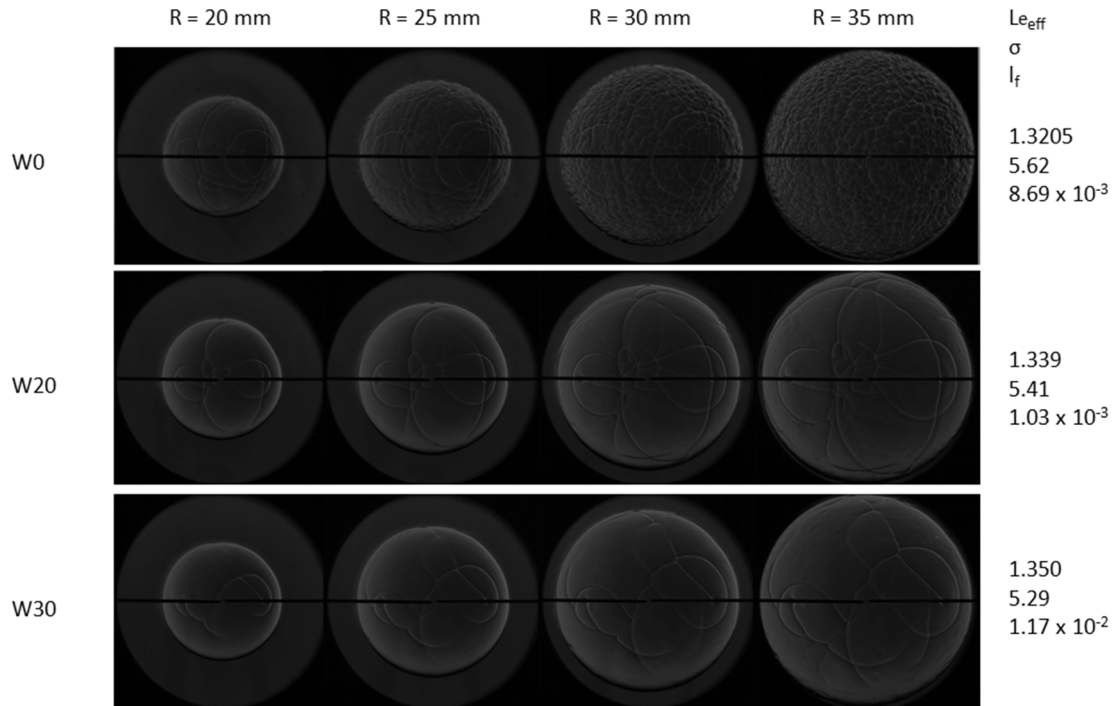


Fig. 12. Schlieren images of stoichiometric ethanol/air mixture, W0, and stoichiometric ethanol-water/air mixtures, W20 and W30, flame front evolution at  $T_u = 450$  K and  $P_0 = 5$  bar. Optical window radius of 35 mm.

with the increase of  $T_u$  as well. This last result is due to the combined effect of a slight decrease of  $Le_{eff}$  with the increase in  $T_u$ , thus increasing the propensity of diffusional-thermal instabilities and suggests that the destabilizing effect, associated with the reduction of the flame thickness, is slightly stronger than the stabilizing effect due to thermal expansion ratio reduction. A similar tendency for initial temperature has been reported for methanol/air [32], though for 2-methyl-1-butanol/air mixtures the flame front stability is reported to be insensitive to  $T_u$  [68].

## 5. Conclusions

The present study investigated the stability of hydrous ethanol/air flames. The effect of flame parameters, such as thermal expansion rate, flame thickness, activation energy, and effective Lewis numbers, on flame dynamics was systematically investigated at various water dilution contents (0 to 30% in volume) and equivalence ratios (0.6 to 1.3), as well as at elevated pressures (2 to 6 bar) and temperatures (380 and 450



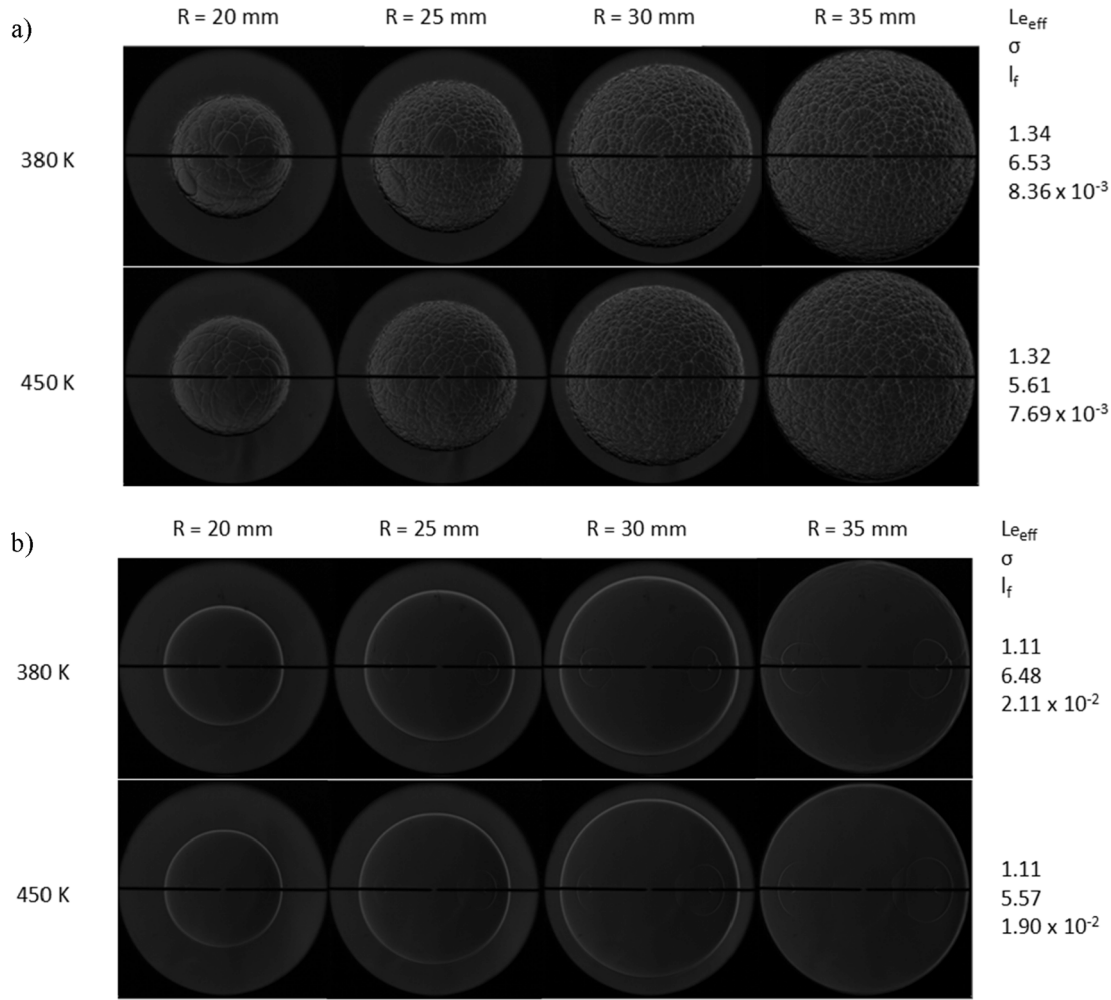


**Fig. 13.** Schlieren images of ethanol/air mixture, W0, flame front evolution for  $T_u = 380$  K and 450 K at: a)  $P_0 = 6$  bar,  $\phi = 1.0$  and b)  $P_0 = 2$  bar,  $\phi = 1.3$ . Optical window radius of 35 mm.

**Table 2**

Critical flame radius,  $R_{cr}$ , for  $P_0 = 2, 4, 5$ , and 6 bar, at W0 and  $\phi = 1.0$ .

$P_0$ (bar)	$T_u$ (K)	$R_{cr}$ (mm)
2	450	Out of visible radius
4	450	Out of visible radius
5	450	28.3
6	380	28.8
6	450	27.5

K). The main results are summarized as follows:

1. The equivalence ratio has a significant effect on flame stability. Slightly rich mixtures present the maximum thermal expansion ratio and minimum flame thickness, thereby, presenting the highest propensity for hydrodynamic instability of the flame front. Besides, the  $Le_{eff}$  significantly decreases by  $\phi$  showing a higher propensity of diffusional-thermal instability for rich mixtures.
2. The addition of water to the ethanol/air mixture leads to a significant decrease in cellular instability. The increase in water content reduces the thermal expansion ratio at all equivalence ratios while increasing the flame thickness almost linearly with the water content, thereby reducing the propensity of hydrodynamic instability appearance on the flame front. Moreover, the increase in water content increases the  $Le_{eff}$  of the mixture, and therefore, is associated with a more diffusional-thermal stable flame.

3. The cellular instability significantly increases while increasing the initial pressure, which resulted from the enhancement of the hydrodynamic instability due to the significant decrease in flame thickness for all equivalence ratios. Also, the pressure increase is associated with mixture  $Le_{eff}$  decrease far from the stoichiometry with a more relevant decrease on the rich side where the propensity of diffusional-thermal instabilities on the flame front is increased.
4. The initial temperature has a weaker effect on cellular instability compared to the other thermo-chemical properties investigated. However, the flame front instability slightly increases with  $T_u$ . Temperature increase leads to a simultaneous reduction of the thermal expansion ratio and flame thickness. The effect of the two parameters almost cancel each other out, thereby explaining the small sensitivity of hydrodynamic instability to  $T_u$ . Besides,  $Le_{eff}$  slightly decreases with mixture temperature and this effect is more pronounced for leaner mixtures, associated with a less diffusional-thermal stable flame.

#### CRediT authorship contribution statement

**Luis Fernando Marcondes Gárzon Lama:** Collected the data, Contributed data or analysis tools, Performed the analysis. **Loreto Pizutti:** Contributed data or analysis tools, Performed the analysis, Wrote the paper. **Julien Sotton:** Collected the data, Contributed data or analysis tools. **Cristiane Aparecida Martins:** Contributed data or analysis tools, Performed the analysis, Wrote the paper.

## Declaration of Competing Interest

The authors declare that they have no known competing financial interests or personal relationships that could have appeared to influence the work reported in this paper.

## Acknowledgments

The authors would like to thank Dr. Ekaterina Mazanchenko and Dr. Alain Clavier for their generous support during the experimental tests. Also, the authors are grateful to the Brazilian agency CAPES which provided funding for mobility via the International Cooperation projects BRAFITEC 214/17 and CAPES-PRINT (Project: Sustainable Energy 88887.310457/2018-00).

## Appendix A. Supplementary data

Supplementary data to this article can be found online at <https://doi.org/10.1016/j.fuel.2020.119555>.

## References

- [1] "Directive (EU) 2018/2001 of the European Parliament and of the Council on the promotion of the use of energy from renewable sources," Off. J. Eur. Union, vol. 2018, no. L 328, pp. 82–209, 2018.
- [2] R. F. Sawyer, "Science based policy for addressing energy and environmental problems," *Proc. Combust. Inst.*, vol. 32 I, no. 1, pp. 45–56, 2009.
- [3] Veloo PS, Wang YL, Egolfopoulos FN, Westbrook CK. A comparative experimental and computational study of methanol, ethanol, and n-butanol flames. *Combust. Flame* 2010;157(10):1989–2004.
- [4] Tao L, et al. "Techno-economic analysis and life-cycle assessment of cellulosic isobutanol and comparison with cellulosic ethanol and n-butanol", *Biofuels*. *Bioprod. Biorefining* 2014;6(3):246–56.
- [5] M. Del Pecchia V. Pessina F. Berni A. d'Adamo S. Fontanesi Gasoline-ethanol blend formulation to mimic laminar flame speed and auto-ignition quality in automotive engines *Fuel* 264 August 2020 2019, p. 116741.
- [6] Bradley D. Combustion and the design of future engine fuels. *Proc. Inst. Mech. Eng. Part C J. Mech. Eng. Sci.* 2009;223(12):2751–65.
- [7] Park K, Choi Y, Kim C, Oh S, Lim G, Moriyoshi Y. Performance and exhaust emission characteristics of a spark ignition engine using ethanol and ethanol-reformed gas. *Fuel* 2010;89(8):2118–25.
- [8] Mack JH, Aceves SM, Dibble RW. Demonstrating direct use of wet ethanol in a homogeneous charge compression ignition (HCCI) engine. *Energy* 2009;34(6):782–7.
- [9] Fagundez JLS, Sari RL, Mayer FD, Martins MES, Salau NPG. Determination of optimal wet ethanol composition as a fuel in spark ignition engine. *Appl. Therm. Eng.* 2017;112:317–25.
- [10] Saxena S, Schneider S, Aceves S, Dibble R. Wet ethanol in HCCI engines with exhaust heat recovery to improve the energy balance of ethanol fuels. *Appl. Energy* 2012;98:448–57.
- [11] Saxena S, Vuilleumier D, Kozarac D, Kriek M, Dibble R, Aceves S. Optimal operating conditions for wet ethanol in a HCCI engine using exhaust gas heat recovery. *Appl. Energy* 2014;116:269–77.
- [12] Liu F, et al. Numerical study and cellular instability analysis of E30-air mixtures at elevated temperatures and pressures. *Fuel* 2020;271:30–2.
- [13] Cai X, Wang J, Bian Z, Zhao H, Zhang M, Huang Z. Self-similar propagation and turbulent burning velocity of CH<sub>4</sub>/H<sub>2</sub>/air expanding flames: Effect of Lewis number. *Combust. Flame* 2020;212:1–12.
- [14] Zhang X, Huang Z, Zhang Z, Zheng J, Yu W, Jiang D. Measurements of laminar burning velocities and flame stability analysis for dissociated methanol-air-diluent mixtures at elevated temperatures and pressures. *Int. J. Hydrogen Energy* 2009;34(11):4862–75.
- [15] Bradley D, Lawes M, Mansour MS. Explosion bomb measurements of ethanol-air laminar gaseous flame characteristics at pressures up to 1.4 MPa. *Combust. Flame* 2009;156(7):1462–70.
- [16] Bradley D, Lawes M, Liao S, Saat A. Laminar mass burning and entrainment velocities and flame instabilities of i-octane, ethanol and hydrous ethanol/air aerosols. *Combust. Flame* 2014;161(6):1620–32.
- [17] Zhang X, Tang C, Yu H, Huang Z. Flame-front instabilities of outwardly expanding iso-octane/n-butanol blend-air flames at elevated pressures. *Energy Fuels* 2014;28(3):2258–66.
- [18] Vu TM, Park J, Kwon OB, Bae DS, Yun JH, Keel SI. Effects of diluents on cellular instabilities in outwardly propagating spherical syngas-air premixed flames. *Int. J. Hydrogen Energy* 2010;35(8):3868–80.
- [19] Gülder ÖL. Laminar burning velocities of methanol, ethanol and iso-octane-air mixtures. *Symp. Combust.* 1982;19(1):275–81.
- [20] Z. K. and C. Q. Liao, S Y, Jiang DM, Huang ZH, "Determination of the laminar burning velocities for mixtures of ethanol and air at elevated temperatures," *Appl. Therm. Eng.*, vol. 27, pp. 374–380, 2007.
- [21] Eisazadeh-Far K, Moghaddas A, Al-Mulki J, Metghalchi H. Laminar burning speeds of ethanol/air/diluent mixtures. *Proc. Combust. Inst.* 2011;33(1):1021–7.
- [22] Egolfopoulos FN, Du DX, Law CK. A study on ethanol oxidation kinetics in laminar premixed flames, flow reactors, and shock tubes. *Symp. Combust.* 1992;24(1):833–41.
- [23] Konnov AA, Meuwissen RJ, De Goey LPH. The temperature dependence of the laminar burning velocity of ethanol flames. *Proc. Combust. Inst.* 2011;33(1):1011–9.
- [24] C. Xu et al., "Combustion Characteristics and Laminar Flame Speed of Premixed Ethanol-Air Mixtures with Laser-Induced Spark Ignition," pp. 63–72, 2017.
- [25] Broustail G, Seers P, Halter F, Moréac G, Mounaim-rousselle C. Experimental determination of laminar burning velocity for butanol and ethanol iso-octane blends. *Fuel* 2011;90(1):1–6.
- [26] Sileghem L, Alekseev VA, Vancoillie J, Nilsson EJK, Verhelst S, Konnov AA. Laminar burning velocities of primary reference fuels and simple alcohols. *Fuel* 2014;115:32–40.
- [27] Dirrenberger P, et al. Laminar burning velocity of gasolines with addition of ethanol. *Fuel* 2014;115:162–9.
- [28] J. Beekmann, O. Röhl, and N. Peters, "Experimental and Numerical Investigation of Iso-Octane, Methanol and Ethanol Regarding Laminar Burning Velocity at Elevated Pressure and Temperature," *SAE Tech. Pap. Ser.*, vol. 1, 2009.
- [29] L. van Treek, M. Lubrano Lavadera, L. Seidel, F. Mauss, and A. A. Konnov, "Experimental and modelling study of laminar burning velocity of aqueous ethanol," *Fuel*, vol. 257, no. July, p. 116069, 2019.
- [30] N. Hinton, R. Stone, R. Cracknell, and C. Olm, "Aqueous ethanol laminar burning velocity measurements using constant volume bomb methods," *Fuel*, vol. 214, no. October 2017, pp. 127–134, 2018.
- [31] L. Garzón Lama J. Sotton C.A. Martins Experimental burning velocities of ethanol-water-air at elevated pressure and temperature *Fuel* 265 December 2020 2019, p. 116933.
- [32] Wang G, Li Y, Li L, Qi F. Experimental and theoretical investigation on cellular instability of methanol/air flames. *Fuel* 2018;225:95–103.
- [33] Gu X, Li Q, Huang Z, Zhang N. Measurement of laminar flame speeds and flame stability analysis of tert-butanol-air mixtures at elevated pressures. *Energy Convers. Manag.* 2011;52(10):3137–46.
- [34] Hu E, Huang Z, He J, Zheng J, Miao H. Measurements of laminar burning velocities and onset of cellular instabilities of methane-hydrogen-air flames at elevated pressures and temperatures. *Int. J. Hydrogen Energy* 2009;34(13):5574–84.
- [35] Bradley D, Lawes M, Mansour MS. Explosion bomb measurements of ethanol – air laminar gaseous flame characteristics at pressures up to 1.4 MPa. *Combust. Flame* 2009;156(7):1462–70.
- [36] Matalon M. Intrinsic Flame Instabilities in Premixed and Nonpremixed Combustion. *Annu. Rev. Fluid Mech.* 2006;39(1):163–91.
- [37] Mitani T, Williams FA. Studies of cellular flames in hydrogen oxygen nitrogen mixtures. *Combust. Flame* 1980;39(2):169–90.
- [38] Williams FA. *Combustion Theory*, Second. 1985.
- [39] Qiao L, Kim CH, Faeth GM. Suppression effects of diluents on laminar premixed hydrogen/oxygen/ nitrogen flames. *Combust. Flame* 2005;143(1–2):79–96.
- [40] Lapalme D, Halter F, Mounaim-Rousselle C, Seers P. Characterization of thermodynamic and hydrodynamic mechanisms on the cellular instability of syngas fuel blended with CH<sub>4</sub> or CO<sub>2</sub>. *Combust. Flame* 2018;193:481–90.
- [41] G. Darrieus, "Propagation d'un front de flamme, presented at La Technique Moderne," *La Tech. Mod.*, p. 1938, 1938.
- [42] L. Landau, "On the theory of slow combustion", *Acta Physicochim. URSS* 19: 77 (1944), vol. 77, p. 1944, 1944.
- [43] Matalon M. The Darrieus-Landau instability of premixed flames. *Fluid Dyn. Res.* 2018;50(5):69–73.
- [44] Sivashinsky GI. Instabilities, Pattern Formation, and Turbulence in Flames. *Annu. Rev. Fluid Mech.* 1983;15(1):179–99.
- [45] Xie Y, Wang J, Xu N, Yu S, Zhang M, Huang Z. Thermal and Chemical Effects of Water Addition on Laminar Burning Velocity of Syngas. *Energy Fuels* 2014;28(5):3391–8.
- [46] Law CK, Sung CJ. Structure, aerodynamics, and geometry of premixed flamelets. *Prog. Energy Combust. Sci.* 2000;26(4):459–505.
- [47] Zhou Q, Cheung CS, Leung CW, Li X, Huang Z. Effects of diluents on laminar burning characteristics of bio-syngas at elevated pressure. *Fuel* 2019;248(March): 8–15.
- [48] Law CK, Kwon OC. Effects of hydrocarbon substitution on atmospheric hydrogen-air flame propagation. *Int. J. Hydrogen Energy* 2004;29(8):867–79.
- [49] Esclapez L. Doctoral Thesis, Numerical Study of Ignition and Inter-Sector Flame Propagation in Gas Turbine. L'Université De Toulouse 2015.
- [50] Bradley D, Hicks RA, Lawes M, Sheppard CGW, Woolley R. The measurement of laminar burning velocities and Markstein numbers for iso-octane-air and iso-octane-n-heptane-air mixtures at elevated temperatures and pressures in an explosion bomb. *Combust. Flame* 1998;115(1–2):126–44.
- [51] Kwon OC, Rozenchan G, Law CK. Cellular instabilities and self-acceleration of outwardly propagating spherical flames. *Proc. Combust. Inst.* 2002;29(2):1775–83.
- [52] Goodwin DG, Moffat HK, Speth RL, An C. "Cantera: An object-oriented software toolkit for chemical kinetics, thermodynamics, and transport processes. 2017; Version 2.3.0. <https://doi.org/10.5281/zenodo.170284>."
- [53] Ansys Chemkin 19.0, "ANSYS CHEMKIN 17.0 (15151), ANSYS Reaction Design: San Diego, 2016," no. December, pp. 1–274, 2016.
- [54] Burali N, Lapointe S, Bobbitt B, Blaquart G, Xuan Y. Assessment of the constant non-unity Lewis number assumption in chemically-reacting flows. *Combust. Theory Model.* 2016;20(4):632–57.

- [55] D. Dandy, "Bioanalytical Microfluidics Program," Color. State Univ. <http://navier.engr.colostate.edu/index.html>, no. February, 2020.
- [56] Beeckmann J, et al. Propagation speed and stability of spherically expanding hydrogen/air flames: Experimental study and asymptotics. *Proc. Combust. Inst.* 2017;36(1):1531–8.
- [57] Matalon M, Cui C, Bechtold JK. Hydrodynamic theory of premixed flames: Effects of stoichiometry, variable transport coefficients and arbitrary reaction orders. *J. Fluid Mech.* 2003;487(487):179–210.
- [58] Bechtold JK, Matalon M. The dependence of the Markstein length on stoichiometry. *Combust. Flame* 2001;127(1–2):1906–13.
- [59] Peters N, Williams FA. The asymptotic structure of stoichiometric methane-air flames. *Combust. Flame* 1987;68(2):185–207.
- [60] Bradley D, Hicks RA, Lawes M, Sheppard CGW, Woolley R. The Measurement of Laminar Burning Velocities and Markstein Numbers for Iso-octane – Air and Iso-octane – n- Heptane – Air Mixtures at Elevated Temperatures and Pressures in an Explosion Bomb. *Combust. Flame* 1998;115:126–44.
- [61] Kwon OC, Faeth GM. Flame/stretch interactions of premixed hydrogen-fueled flames: Measurements and predictions. *Combust. Flame* 2001;124(4):590–610.
- [62] Bradley D, Cresswell TM, Puttock JS. Flame acceleration due to flame-induced instabilities in large-scale explosions. *Combust. Flame* 2001;124(4):551–9.
- [63] Kwon OB, Keel SI, Bae DS, Park J, Vu TM, Yun JH. Effects of diluents on cellular instabilities in outwardly propagating spherical syngas–air premixed flames. *Int. J. Hydrogen Energy* 2010;35(8):3868–80.
- [64] Law CK, Jomaas G, Bechtold JK. Cellular instabilities of expanding hydrogen/propane spherical flames at elevated pressures: Theory and experiment. *Proc. Combust. Inst.* 2005;30(1):159–67.
- [65] R. Le Dortz, M. Bellenoue, and S. Julien, "Effects of Pressure and Temperature on Laminar Burning Velocity of a Kerosene Surrogate," in 26 th ICEDERS July-August, 2017, 2017, no. September.
- [66] R. Le Dortz, "Détermination des caractéristiques fondamentales de combustion de pré-mélange air-kérosène, de l'allumage à la vitesse de flamme : représentativité de surrogates mono et multi-composants," l'École Nationale Supérieure de Mécanique et d'Aérotechnique, 2018.
- [67] Varea E, Modica V, Renou B, Boukhalfa AM. Pressure effects on laminar burning velocities and Markstein lengths for Isooctane-Ethanol-Air mixtures. *Proc. Combust. Inst.* 2013;34(1):735–44.
- [68] Li Q, Hu E, Cheng Y, Huang Z. Measurements of laminar flame speeds and flame instability analysis of 2-methyl-1-butanol-air mixtures. *Fuel* 2013;112:263–71.